

Thesis for the degree of Licentiate of Technology
Sundsvall 2017

Measuring Water Droplets to Detect Atmospheric Icing

Staffan Rydblom

Supervisor: Associate Professor Benny Thörnberg,
Professor Mattias O'Nils

Department of Electronics Design, in the
Faculty of Science, Technology and Media
Mid Sweden University, SE-851 70 Sundsvall, Sweden

ISSN XXXX-XXXX

ISBN XXXX-XXXX

Mid Sweden University Licentiate Thesis XX



Akademisk avhandling som med tillstånd av Mittuniversitetet i Sundsvall framläggs till offentlig för avläggande av licentiatexamen i elektronik **onsdagen den 1 november 2017, klockan ??:00 i sal ??**, Mittuniversitetet Sundsvall. Seminariet kommer att hållas på engelska.

Measuring Water Droplets to Detect Atmospheric Icing

Staffan Rydbom

©Staffan Rydbom, 2017

Electronics Design Division, in the Faculty of Science, Technology and Media Mid Sweden University, SE-851 70 Sundsvall Sweden

Telephone: +46 (0)60 148422

Printed by Kopieringen Mittuniversitetet, Sundsvall, Sweden, 2017

For Sara, Alva and Ludvig. <3

ABSTRACT

This thesis describes the exploration of a method to measure the droplet size and the concentration of atmospheric liquid water. The purpose is to find a cost efficient technique to detect the conditions for icing on structures.

Icing caused by freezing atmospheric water can be a significant problem for infrastructure such as power lines, roads and air traffic. About one third of the global installed wind power capacity is considered to be in cold climates, where icing of rotor blades is one of the major challenges.

The icing process is complex and the result depends on a combination of the aerodynamic shape of the structure or airfoil, the velocity of the air and its contained water, the temperature, the mixing of snow and water, the concentration of liquid water and the droplet size distribution.

The chosen measurement method is based on a shadowgraph imaging system using LED light as background illumination and digital image processing. A prototype instrument is constructed. The components are chosen with the possibility of low cost volume production in mind. The applications of a commercial instrument based on this technique are e.g. real-time in-situ icing condition measurements and assimilation and verification of data in numerical weather models.

The work presented shows that measurements of the size and concentration of water droplets using shadowgraph images can be used for the comparison and validation of NWP (Numerical Weather Prediction) models and other instruments. The accuracy of the particle size measurement is high. The accuracy of the concentration measurement has the potential to become high due to the single-particle measurement range calibration. The precision of the instrument depends mainly on the number of images that is used to achieve each measurement value. The real-time performance of the instrument is limited by the image retrieval and processing speed and depends on the precision required.

SAMMANFATTNING

Den här avhandlingen beskriver utforskandet av en metod att mäta storlek och koncentration av vattendroppar i atmosfären. Avsikten är att hitta en kostnadseffektiv teknik för att förutsäga isbildning.

I bildning som orsakas av atmosfäriskt vatten kan vara ett signifikant problem för vår infrastruktur som t.ex. kraftledningar, vägar och flygtrafik. Omkring en tredjedel av den globala installerade vindkraften anses vara i kalla klimat, där nedisning av rotorbladen är en av de största utmaningarna.

Nedisningsprocessen är komplex och resultatet beror på en kombination av strukturen eller vingens aerodynamiska form, den förbi passerande luftens hastighet, luftens och ytans temperatur, eventuell blandning av snö och vatten, concentrationen av flytande vatten och dessa vattendroppars storleksdistribution.

Den valda mätmetoden baseras på skuggfotografering med en LED som bakgrundsbelysning samt digital bildbehandling. Ett prototypinstrument är konstruerat med övervägande standardkomponenter. Dessa har valts med tanke på möjligheten till låg produktionskostnad. Exempel på applikationer för ett kommersiellt instrument baserat på denna teknik är villkorsmätning för nedisning i realtid, assimilation och verifikation av data i numeriska vädermodeller.

Arbetet som presenteras visar att mätning av storlek och koncentration av vattendroppar med hjälp av skuggfotografering kan användas för validering av NWP-modeller och andra instrument. Noggrannheten hos storleksmätningen är hög. Noggrannheten av koncentrationsmätningen har potential att bli hög eftersom varje droppe får en individuellt kalibrerad mätvolym. Precisionen hos mätinstrumentet beror till största delen på hur många bilder och vattendroppar som används för att skapa varje mätvärde. Instrumentets prestanda för att mäta i realtid begränsas av kamerans bildhastighet och bildbehandlingstiden samt vilken precision i mätvärdet som önskas.

CONTENTS

ABSTRACT	v
SAMMANFATTNING	vii
CONTENTS	viii
LIST OF FIGURES	x
LIST OF TABLES	xii
LIST OF PAPERS	xiii
ACKNOWLEDGEMENT	xv
1 INTRODUCTION	1
1.1 Atmospheric Water and Icing	1
1.2 Justification and Narrative	3
1.3 Related Work of Measurement	4
2 THEORY	7
2.1 Forming of Ice	7
2.2 Liquid Water Content and Median Volume Diameter	8
2.3 Practical Problems with Measuring Atmospheric Water	9
2.4 Light Scattering and Absorption	10
3 MATERIALS AND METHODS	13
3.1 The Shadowgraph System	13
3.2 Image Segmentation	15
3.3 Design Considerations	23
3.4 Calibration and Validation of the Calibration	23
3.5 The Fog Chamber	25
3.6 The Klövsjö Installation	26
3.7 Numerical Weather Prediction	28

Contents

4 RESULTS	31
4.1 Measurement of Polymer Microspheres	31
4.2 Comparison of DII and CDP Data	32
4.3 Comparison of Measured and Modeled Data	33
5 DISCUSSION	37
5.1 Starting Studies	37
5.2 Aerodynamics	39
5.3 Difficulties with Polymer Microspheres	39
5.4 LED Illumination	41
5.5 Statistics	41
5.6 Droplets and Size Distributions	41
5.7 Icing	44
6 SUMMARY OF THE THESIS	47
6.1 General Conclusions	47
6.2 Other Conclusions	47
6.3 Future Work	48
6.4 Authors' Contributions	49
BIBLIOGRAPHY	51

LIST OF FIGURES

2.1	Supercooled water droplets on collision course with an aerodynamic profile.	8
3.1	Principle of shadowgraphy. 1. Camera. 2. Telecentric lens. 3. Parallel focused light beam. 4. Collimating lens. 5. LED.	14
3.2	The experimental setup with a dot micrometer scale as test object mounted on a translation stage.	14
3.3	The illumination and detector is mounted inside two Bosch camera housings facing each other with heating inside the house and on the front glass.	15
3.4	Same dot viewed in different background light. 455 nm (left) and 850 nm (right).	20
3.5	Spectrum of the Mightex 455nm LED using two different driving currents. The band width is slightly wider for the higher current.	20
3.6	SNR for a ten micrometer dot image using two wavelengths and seven gain level settings. Shorter wavelength and lower gain gives less noise.	21
3.7	Mean pixel value and standard deviation of ambient for a light measurement at 22000 lux.	22
3.8	Light energy (nJ) for exposure in each of the eight gain levels used. The energy was tuned manually up to a level of high exposure, but not saturating any point in the image.	23
3.9	Measuring range (mm) vs. diameter for two different thresholds (0.005 and 0.002).	24
3.10	The 50 micrometer dot with front illumination imaged using 40x magnifying lens.	25
3.11	Fog chamber with connected droplet generator (blue container) and a multimeter used for fan power measurement. A Beaglebone Black microcontroller (blue box) is used for fan speed regulation.	27

3.12	Icing on the front side of the installed instruments.	27
3.13	Installation in Klövsjö.	28
3.14	Graphical presentation of data from the HARMONIE-AROME weather model covering Klövsjö and the surrounding mountains at a specific point in time using 500 m resolution. Yellow areas are where the model predicts an LWC more than $0.1 \text{ g} \cdot \text{kg}^{-1}$ (Grams of water per kg air.) Simulation and figure by SMHI.	29
4.1	Histograms of the four measured distributions. The dashed line is a fitted lognormal of the weighted distribution.	31
4.2	LWC measured by the DII and the CDP for 46 hours on 28-02-2017–01-03-2017.	32
4.3	MVD minute values measured by the DII and the CDP for 46 hours on 28-02-2017–01-03-2017.	33
4.4	Relation between the wind speed and the quote between the LWC measured by the CDP and the DII. The vertical scale is cropped at 1 and 100. 238 values are above 100 and 121 below one out of a total of 2760.	33
4.5	LWC and MVD measured by the DII and the CDP 11-12-2016. HARMONIE-AROME model data using 500 meter resolution.	34
4.6	LWC and MVD measured 03-02-2017–06-02-2017 by the DII. HARMONIE-AROME model data using 2.5 km resolution, stored every 60 minutes.	35
4.7	LWC and MVD measured by the DII and the CDP 10-02-2017. HARMONIE-AROME model data using 2.5 km resolution, stored every 60 minutes.	35
5.1	A 74 μm droplet detected at 04:41 on 05-02-2017.	44
5.2	Two droplets, 19 and 62 μm in diameter detected in the same image at 16:48 on 05-02-2017.	44

LIST OF TABLES

3.1	Micro dot verification measurement. All values are in μm . Eccentricity is here the maximum difference in μm between the smallest and the largest measured diameter.	26
4.1	Summary of the result from the measurement of NIST certified microspheres. All values are in μm	32
6.1	MA = Main Author, CA = Co-Author, PM = Project Member, LC = Language Check.	50

LIST OF PAPERS

This thesis is based on the following papers, herein referred to by their Roman numerals:

PAPER I

- Liquid Water Content and Droplet Sizing Shadowgraph Measuring System for Wind Turbine Icing Detection
S.Rydblom, B. Thörnberg, IEEE Sensors Journal, 2015 ??

PAPER II

- Droplet Imaging Instrument - Metrology Instrument for Icing Condition Detection
S.Rydblom, B. Thörnberg, IEEE International Conference on Imaging Systems and Techniques (IST) Proceedings, 2016 .. ??

PAPER III

- Comparative Field Study of LWC and MVD using two Droplet Measuring Instruments and a NWP Model
S.Rydblom, B. Thörnberg, E. Olsson, Under Review for Cold Regions Science and Technology, 2017 ??

ACKNOWLEDGEMENT

I would like to express the greatest gratitude to my supervisor, Benny Thörnberg, for his trust and encouragement during hard times when things did not turn out the way they were expected. I would also like to thank Mattias O'Nils and Claes Mattsson at the Electronics Department for making the project possible and giving me the possibility to finish the thesis. A big thank is also given to the Swedish Energy Agency for funding most of the work, Patrik Jonsson, Björn Ollars and Olof Carlsson at Combitech for their invaluable work with integrating the CDP and Esbjörn Olsson at SMHI for sharing his knowledge about the weather physics and his work with the NWP model data. The greatest love and gratitude towards my wonderful family that have sacrificed and supported me in beginning, fulfilling and finishing this work. Without you this would not have been possible. Special thanks to Lotta Frisk for chasing my signatures, Fanny Burman for the dances, Carolina Blomberg for the skis, Christine Grafström for the run and Maria Rumm for SMART inspiration. I would also express my gratitude to my mentor Magnus Göran Tungström, David Kraphol, Kent Bertilsson, Henrik Andersson, Javier Brugés, Igor Fedorov, Jan Thim, Enkeleda Balliu, Muhammad Abu Bakar, Amir Yousuf and Johan Sidén for support and fruitful discussions. Lisa Velander for language correction. All the people at Mid Sweden University.

— Chapter 1 —

INTRODUCTION

This thesis describes the exploration of a method to measure the size and concentration of atmospheric liquid water, with the purpose of finding a cost efficient technique to detect the conditions for icing on structures. The chosen measurement method is based on digital image processing and a shadowgraph imaging system using LED light as background illumination. A prototype instrument is manufactured using components with the intent of viewing possibilities of low cost volume production. The applications of a commercial instrument based on this technique are e.g. real-time in-situ icing condition measurements and assimilation and verification of data in numerical weather models.

Paper I describes a shadowgraph system that uses edge detection to define a measurement range depending on the size of a particle and the image signal to noise ratio (SNR). Paper II describes the design of the weather protected prototype and a fog chamber used for climate tests. Paper III describes a verification of the size measurement using polymer microspheres in calibrated (NIST traceable) distributions and a field study of ground LWC and MVD using the DII and a comparative study using the Cloud Droplet Probe (CDP).

1.1 Atmospheric Water and Icing

Measuring or controlling the properties of a fog of water droplets has been the interest and focus of many studies during at least half a century. Applications can be found in many different fields, like atmospheric studies, aircraft and road traffic safety, medicin, infrastructure and military defence. When a mass of air is saturated with water vapour the abundant water will be in either liquid or solid form. In order to for water to freeze, or change from liquid to solid state, it needs to be below zero degrees Celsius at the standard atmospheric pressure (273.15 K at 101.325 kPa). For an ice crystal to form in the atmosphere, unless the temperature is below -40°C, the presence of an ice nucleus is also required. If no ice nucleus is present,

the water droplet will remain in the liquid but supercooled condition. In this condition the water freeze very quickly on the contact with a cold surface. Depending on the size of the droplets, the icing is called in-cloud icing, freezing rain or wet snow icing. Combinations of these weather conditions are common.

Icing caused by freezing atmospheric water can be a significant problem in cold climates, affecting infrastructure such as wind turbines, power lines, road and air traffic. With the increasing importance of electric power generated by wind, there is a demand for predictions of icing on wind turbines. Icing on the blades of a turbine lowers the efficiency, increases noise and may force the turbine to a complete stop [15, 20, 29, 32]. Aircraft, power lines or any other weather exposed structure share this problem. Efforts have been made to create models for how the ice is formed [45, 47, 61] and how it can be included in weather prediction models [64, 39]. The severity of the icing depends on many factors, e.g. the duration, the shape and surface of the structure, the wind speed, the atmospheric concentration of liquid water, the size distribution of water droplets and the mix of ice and snow [39, 45, 47, 28, 25]. Of particular interest for the prediction of effect loss on a wind turbine is the phase of ice accretion [davis2013].

The Liquid Water Content (LWC) in atmospheric studies is usually given in either $\text{g} \cdot \text{m}^{-3}$ [59] or as the mass quote of water and air $\text{g} \cdot \text{kg}^{-1}$. The size distribution of droplets when considering the collision efficiency is most effectively estimated by the Median Volume Diameter (MVD) [21]. The MVD is the point in the distribution of droplet diameters where half of the total amount of water in the distribution of droplets is above the diameter, while the other half is below. Weather models today include the LWC and the MVD, making it possible to estimate the risk of icing based on general weather data [64]. The LWC and the MVD at ground level depends very much on the local geographical topology, and measurements using in situ instruments are quite rare. There have been trials to verify NWP models using in-situ data [6]. The LWC and the MVD e.g. can be measured by analyzing satellite or radar images. In-situ measurements are rarely simple or straightforward, especially considering the occurrence of mixed conditions mentioned. Despite the development of diverse measurement techniques and instruments, in-situ measurements are

still quite rare due to the cost and that most instruments require more or less installation expertise, maintenance and periodic calibration.

1.2 Justification and Narrative

Regions where icing events or periods with temperatures below the standard operational limits occur are of great interest for the installation of wind power. About one third of the global installed wind power capacity is considered to be in these cold climates, where icing of rotor blades is one of the major challenges [9].

The work leading to this thesis started with an open mindset and the goal set to find a method to detect icing on wind turbines by measuring the optical properties of liquid water in clouds. We knew from previous projects how the reflectance and absorbtion of light changes depends on the wavelength. The absorption of light is comparatively high for some wavelengths in near and far infrared, but low in the visible blue and green. Clouds consist of water droplets, but the absorption is a function of the travelled distance, which makes it very small in small droplets. Most of the light will be scattered, which is why clouds appear gray at a distance. Light with strong coherence, like that from lasers, will be affected by interference. Coherent and incoherent light sources in wavelengths from visible (450 nm) to near infrared (850 nm) were tested. Illumination angles were tested from 90 (sideways) to 180 (backlit) degrees. After evaluating the different techniques, 180 degrees backlit illumination using blue LED was selected.

Optical measurement of water droplets have been researched and resulted in many publications during the last decades. Shadowgraphy is also used in particle velocimetry, for analyzing sprays in many different applications. Therefore there are many publications and litterature available on these subjects. Still, there is no instrument readily available today that is affordable, reliable and possible to operate near the highest point where icing usually occur, like a hundred meters up in a wind turbine, or mast. An instrument for measuring icing parameters for wind turbines should both be able to detect supercooled cloud droplets from five to a few hundred

micrometers in diameter and be able to determine the concentration to get an accurate measure of the LWC.

The Droplet Imaging Instrument (DII) was designed to find a simple, cost effective and robust technique to measure LWC and MVD in order to predict icing on structures. An automatic sensor based on this technique could be used to trigger ice protection systems used for wind turbines in cold climates [lamra2013]. It was calibrated using a micrometer dot scale with dots of verified sizes printed on a transparent glass. The sizing is verified using four samples of polymer microspheres, calibrated in turn by the National Institute of Standards and Technology (NIST). The functional simplicity and robustness of the DII opens the possibility to mass produce and distribute Internet connected instruments based on this technique on a larger geographical scale.

During the winter of 2016-2017, the prototype instrument was placed on the Klövjo mountain, Sweden, at one of the Swedish Meteorological and Hydrological Institute's (SMHI) measuring stations, position $62^{\circ}29'41''\text{N}$, $14^{\circ}9'27''\text{E}$, 802 meters above sea level. Measurements are available from November 2016 to March 2017. Results from this measurement together with a parallel measurement of LWC and MVD using a Cloud Droplet Probe CDP-2 (CDP) from Droplet Measurement Technologies Inc. (DMT) are presented in Paper III as well as in this thesis.

1.3 Related Work of Measurement

Describe shortly the DII (technical data) for comparison?

In 1970, Knollenberg [35] described an electro-optical technique to measure cloud and precipitation particles using a laser illuminated linear array of photo detectors. The photo detectors are used to make a two-dimensional image of the particles' shadows as they pass the light beam. Systems based on this technique are called Optical Array Probes (OAP) or two-dimensional imaging probes. Developments of this technique include using image sensors to save gray scale images of the detected particles [41, 70]. The Droplet Imaging Instrument (DII) developed and described in this thesis is based on this technique.

Light scattered from a focused laser [3, 17] is a different technique to measure single particles. A laser beam is used to illuminate pass-

1.3. Related Work of Measurement

ing particles. When a particle is detected, its size is determined by comparing the variations in light with a pattern derived from the Mie scattering solutions [49]. The Cloud Droplet Probe (CDP) used as a reference instrument is based on that technique.

The OAP, imaging and the light scattering spectrometers each have some advantages over the other technique depending on the nature of the aerosol. Instruments for airborne use have been developed that combine several techniques into one single probe for accurate measuring of LWC and MVD [5, 4].

A similar but different optical technique for measuring water droplets is based on in line holography [42]. In principle this is a two-dimensional shadowgraph imaging system that use laser background illumination to create images of the diffraction patterns created by the passing particles. These patterns are measured to reconstruct images of the particles. This is a fairly calculation intensive process, which may be one of the reasons why instruments based on this technique are not so common yet [26]. An advantage with this technique is the increased measurement range, i.e. the useable depth in each image [33].

Sizing of the droplets using Mie spectrometry is a complex operation even for coherent light citebohr2008, and although it is possible to study Mie scattering from white light [69], the complexity, small droplet size range and sample volume makes it less attractive in this application. The optical resolution is usually too low. Therefore it is also difficult to determine the exact particle size and the usable depth of field for incoherent shadowgraph systems. The shadow from a particle can e.g. appear smaller or larger when out of focus.

Shadowgraph imaging of particles using incoherent illumination instead of laser has been tried e.g. in particle shadow velocimetry (PSV) [18], or spray characterization [72]. Quantitative and comprehensive studies of other droplet measurement techniques exist [17, 26, 14].

Kuhn et. al. [40] described a method to characterize ice particles by Fourier shape descriptors [23, 68]. The system uses a microscope-like technique to achieve a high resolution level, in the order of one micrometer. Although not specifically designed to measure water droplets, the principal design is similar to the DII.

— Chapter 2 —

THEORY

This chapter begins with an introduction to the physics behind the forming of ice on structures. The next two sections briefly describe the measurement parameters and some practical problems of measuring icing. The last section is about scattering of light by small particles.

2.1 Forming of Ice

An icing event can be divided in the incubation, the accretion and the persistence/ablation phase. Atmospheric icing is the period of time where atmospheric conditions are present for the accretion of ice or snow on structures [9]. The icing process is complex and the result depends on a combination of the aerodynamic shape of the structure or airfoil, the velocity of the air and its contained water, the temperature, the mixing of snow and water, the concentration of liquid water and the droplet size distribution.

A particle's eagerness to follow the flow or collide depends on the flow velocity, the size and shape of the obstacle, the density and drag coefficient of the particle. This relationship is known in fluid mechanics as the Stokes number (Stk). Small droplets or particles with $Stk \ll 1$ may continue with the airflow around the profile, while large droplets or particles with $Stk \gg 1$ due to their inertia collide with the structure. A supercooled droplet colliding with a structure would likely freeze on the impact. Figure 2.1 illustrates the difference between large and small supercooled droplets passing an aerodynamic profile.

Icing on wind turbines forms slightly differently from the ice accretion on an aircraft airfoil. Since the turbine is stationary it cannot stop the icing, or de-ice by moving to a different position. The same conditions may persist for days or weeks. The turbine blade moves concentrically making the tip of the blade the fastest, and highest located moving part. There is no status surveillance of the wings. Therefore the remote and exposed position makes it difficult to detect ice directly when it is initially formed [27].

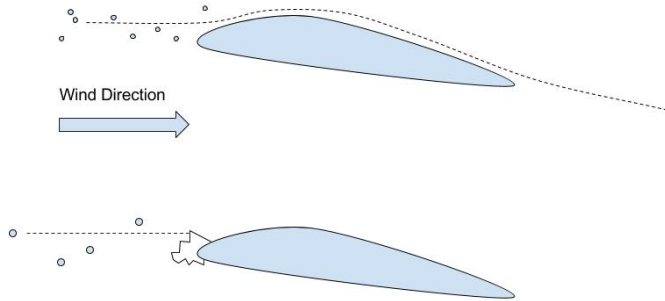


Figure 2.1: Supercooled water droplets on collision course with an aerodynamic profile.

2.2 Liquid Water Content and Median Volume Diameter

The liquid water content (LWC) and the water droplets median volume diameter (MVD) are parameters that can be used to predict or model icing. The MVD is given at the point where half of the total volume of liquid content in a fixed air volume consists of droplets with diameters larger and the other half has smaller diameters. The MVD has been assumed to give the best approximation to the spectrum of diameters in a droplet distribution, when considering the collision efficiency [21]. To estimate the amount of icing created by supercooled water droplets, for most cases the MVD has been shown to be a good indicator [45]. This model using the MVD can also be used for simulating ice accretion on wind turbines [16].

In practice, the LWC and the MVD are scarcely ever measured at a planned or existing wind turbine [53, 44]. Measuring these properties accurately and frequently would be an advantage for the planning of new wind mill farms or for the application of anti-icing arrangements on existing power stations. It may be of particular interest as input to weather prediction models by which both LWC and MVD can be computed [64, 51]. In combination with information about the aerodynamic properties of the wind turbine, it can give more accurate predictions of icing or even result in better design of wind turbines and anti-icing methods.

While icing caused by large supercooled droplets, with diameters

2.3. Practical Problems with Measuring Atmospheric Water

from approximately 50 µm to exceeding 1000 µm, is often considered severe due to its shape and quick build-up, icing may occur even with droplets as small as 5 µm [58, 12, 28]. In most cases, though, icing is caused by cloud droplets measuring between 10 µm and 30 µm in diameter [44, 12].

Although optical imaging and other techniques for measuring aerosol properties is continuously improving, the choice of instrument is still very much dependent on the application's requirements [30, 3, 4, 41]. An instrument for measuring icing parameters for wind turbines should be able to detect supercooled cloud droplets from five micrometer and determine an accurate measure of the LWC. Since measurements are needed in multiple remote locations it should also be affordable, reliable, have low power consumption, and ideally be possible to place near the highest point of the turbine [27].

2.3 Practical Problems with Measuring Atmospheric Water

The varying nature of atmospheric water particles mentioned in the previous chapter makes it very difficult to measure all kinds and sizes of particles using a single instrument. Therefore atmospheric aerosol studies are often done with one or several instruments combining different techniques. Each technique has its limitations and problems. It is also difficult to find a reference sample with the same but known properties as the water. Free floating water droplets tend to be affected by gravity, collide and coalesce, evaporate or stick to any surface.

The size of water droplets range from a few micrometers to several mm in diameter. An imaging instrument is limited by the optical system's resolution, it's field of view and the usable depth of field or the measuring range.

Many existing instruments suffer from errors caused by the instrument itself during sampling, e.g. when droplets get stuck on the inlet [62]. At higher wind speeds particles shatter into smaller droplets or bounce on the supporting structure making up the instrument [13, 19]. All droplets or particles approaching an obstacle are affected by the change in pressure and wind direction surrounding it, a fact which complicates measuring the concentration of particles in unaffected air. Measurement probes working by extraction of air using a mechanical

Chapter 2. Theory

air pump would expect a loss of particles with large Stokes numbers. Ideally the measuring device should be designed in order to affect the free flow of particles as little as possible [4].

An instrument that uses the fact that supercooled water droplets will freeze on the impact, is e.g. the rotating cylinders used by Makkonen [44]. By exposing cylinders of different diameters, depending on the amount of ice accumulated on each cylinder, the MVD and LWC can be calculated from a theoretical model. While this technique provides a nice alternative to the single particle measurements its drawback is that it requires some manual operation and of course the fact that only freezing water can be measured.

Measuring particles from aircraft is partly made complicated by the high air speed. The sample is affected by the change in pressure surrounding the aircraft and by particles hitting parts of the probe, splintering or changing direction, causing anisokinetic sampling [4]. An instrument fixed to the ground on the other hand is affected by the wind speed relative to the ground. This means that it needs to be directed in the direction of the wind. Particles may also enter the measurement zone from different directions depending on their Stokes number, which has been shown to have an effect on the measured liquid water content [26].

Instruments based on Mie calculations of light scattering have sometimes the issue of dealing with a non-linear relation between scattering response and diameter. Aliasing in the sample bin resolution can lead to spikes in the size distribution. Particularly interesting is the 10 to 15 μm range, where two particles with diameters differing more than one micrometer can have the same scattering intensity response [17, 62, 7].

2.4 Light Scattering and Absorption

In visible light, water is almost transparent. This means that the imaginary part of the refractive index, i.e. the absorption, is very small, while for some higher and lower wavelengths it increases with a factor of almost ten power to ten [38]. This fact is used in two-color lidar measurements [71]. The real part of the refractive index for water is much more stable, approximately 1.34 at 455 nm light [24]. For

2.4. Light Scattering and Absorption

simplicity we have assumed that the refractive index of air is equal to one.

A droplet works as a spherical lens with a very short focal length. Exposed to a background illumination it will scatter almost all of the light reaches the droplet in different directions, causing a shadow that appears as a black disc except for the refracted light passing straight through the center. Some of the light will of course be absorbed, albeit the absorption of a single water droplet is negligible due to its small volume and because water absorb very little in the visible spectrum.

When the light source is spread out compared with the size of the droplets, as in the case of using a collimated LED, the intensity of the center Arago spot caused by Fresnel diffraction would be negligible [55].

The combined effect of scattering and absorption is the extinction [7]. Due to this combined effect, clouds look nontransparent from a distance. Measuring extinction is possible in aerosols e.g. by using Raman LIDAR [2].

MATERIALS AND METHODS

Initially different light sources and illumination angles were investigated. It was decided to use a shadowgraph system with background illumination. The experimental setup was tested using different water droplet generators and a test target consisting of micrometer sized lines and dots. Analyzing the optical system and testing different segmentation algorithms we found a simple way to define the sample volume for each individual droplet. To test the ability of measuring concentration we needed to build a weather protected prototype that could be used in parallel with a second instrument. The prototype needed to be fully automatic, able to analyze images in real time 24 hours a day during several months and store the results in a compressed format. To calibrate the size measurement and the measurement range, the previously mentioned dots of different sizes were used. The size measurement was also verified using distributions polymer microspheres, applied by blowing compressed air through a glass dispenser.

3.1 The Shadowgraph System

The instrument is a shadowgraph system using a monochrome CMOS camera with a 4x magnifying telecentric lens and a LED with a collimating lens illuminating the background. The blue LED is powered by a current driver able to produce short 12 A current pulses. Figure figure 3.1 shows a sketch of the system.

The system is mounted in a weather proof shell using two standard camera housings and a separate box for the analyzing computer and power supply. Fig. 2 shows the system mounted in weather proof camera housings.

Calibration of true droplet size and measuring range both depends on the measured size of the droplet shadow and the amount of light

Chapter 3. Materials and Methods

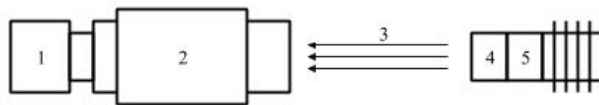


Figure 3.1: Principle of shadowgraphy. 1. Camera. 2. Telecentric lens. 3. Parallel focused light beam. 4. Collimating lens. 5. LED.

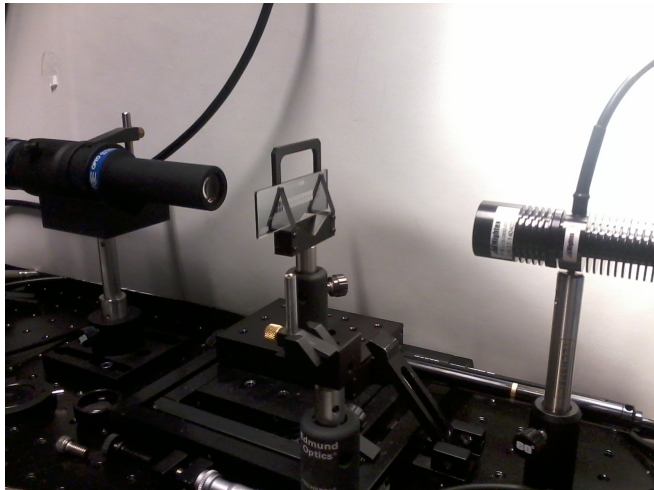


Figure 3.2: The experimental setup with a dot micrometer scale as test object mounted on a translation stage.

used for exposure. It is possible to predict both the precision of the measured size and accuracy for measurement of droplet size.

We used a stage micrometer scale for characterization of the system and simulation of water droplets. This characterization holds true given that the optical silhouette of a droplet is comparable to a dot having equal diameter and being printed on a silicon glass. It is not a new concept and has at least once been proved experimentally, by comparing with beads of glass and water droplets of known sizes [37, 36]. The shadow image of water drops of any size will be defined mainly by the diffracted component, as long as the distance between the drop and the lens is much larger than the drop diameter [37, 70].

The design using a weakly collimated LED that illuminates an area slightly larger than the field of view makes the system quite insensitive

3.2. Image Segmentation



Figure 3.3: The illumination and detector is mounted inside two Bosch camera housings facing each other with heating inside the house and on the front glass.

to misalignment of the camera and the light source. Temporal or permanent changes in light intensity caused by a minor misalignment is automatically compensated for by continuous measurement of the total exposure level. If the level of exposure is increasing or decreasing, the length of the light pulse is changed correspondingly. The light intensity can also be affected by dirt on the front glass of the housings.

Since many images will not contain any droplet at all, we can increase the processing speed by sorting out the images that are not containing any interesting information. This is done by constructing an average image from 20 images and use this as a flat-field correction. All new images are compared with this average and if any pixel differs from the average by more than a specific value that is significantly higher than the noise level, the image is analyzed.

Spatial dissimilarities in the light intensity that are not caused by noise are compensated for by calculating the local average intensity of the background around each measured droplet. The size of a droplet is then based on the intensity dip caused by the shadow compared with its local background.

3.2 Image Segmentation

Detection of patterns in a gray level image can be done in many ways. The easiest method is to use a threshold at a fixed level. The boundary of the pattern can be found in the transition between above and

Chapter 3. Materials and Methods

below that threshold. When the value of the background illumination varies in a systematic pattern, a variable threshold can be used [22]. An average image is constructed by 20 images and used as the base pattern. If any point in this the new image differs enough from this average the image is processed using edge detection. This technique is very fast and is therefore used in this system before the edge detection to sort out images that likely do not contain any interesting information.

If the image contains an object detected by the thresholding, the sample volume is calculated for each droplet individually depending on it's size. By using a Laplacian of Gaussian [48, 22] edge detection and a suitable threshold, we can create closed curves around objects where the edge is in or near focus. Other edge detection operators like Roberts, Prewitt, Sobel [22] and Canny [10] did not seem to give the same consistant performance in different lighting conditions. The objects that create closed curves, selected by a boundary fill function, are said to be within the measuring range. The measuring range together with the field of view defines the sampling volume. This and the edge detection is also described in Paper I. Since the Laplacian of Gaussian can be seen as value of the second derivative of the edge gradient, it is also used together with the diameter to calculate the true size of the droplet as described in Paper II.

3.2.1 Exposure Check and Flash Intensity Adjustment

Let $I_{i,j}$ depict the two dimensional image captured by the camera. The mean value \bar{i} of all pixels in the image $I_{i,j}$ gives an estimation of the exposure level in the whole image.

The flash duration is adjusted automatically by the microcontroller at each exposure to keep the exposure level between a low and a high threshold, th_L and th_H . The duration is changed in steps of 13 ns corresponding to one clock cycle of the microcontroller. If $\bar{i} > th_L$ and $\bar{i} < th_H$ the image is analyzed. If $\bar{i} \geq th_H$ the flash duration is decreased by steps of 12 ns. If $\bar{i} \leq th_L$ the flash duration is increased. The total flash duration is approximately 250 ns. th_L is here set to 0.7 and th_H is set to 0.8 in a normalized (0,1) dynamic range.

3.2.2. Edge Detection and Edge Sharpness

3.2.2 Edge Detection and Edge Sharpness

To detect the intensity changes created by the shadow of a water droplet, an image is processed using the from edge detection theory well known Laplacian of Gaussian (LoG) described by Marr and Hildreth [48]. The method works by looking for zero crossings in the image resulting from calculating $\nabla^2 G(x, y) * I(x, y)$. $G(x, y)$ is a two dimensional Gaussian distribution with standard deviation σ and ∇^2 is the Laplacian operator, defined as the divergence of the gradient in two dimensions.

$$G(x, y) = \frac{1}{\pi\sigma^2} e^{-\frac{x^2+y^2}{2\sigma^2}} \quad (3.1)$$

$$\nabla^2 = \nabla \cdot \nabla = \frac{\delta^2}{\delta x^2} + \frac{\delta^2}{\delta y^2} \quad (3.2)$$

We implement a discrete approximation to $\nabla^2 G(x, y) \approx \nabla^2 G_{i,j}$ as a 13x13 sized convolution kernel.

$$\nabla^2 G_{i,j} = -\frac{1}{\pi\sigma^4} \left(1 - \frac{i^2 + j^2}{2\sigma^2}\right) e^{-\frac{i^2+j^2}{2\sigma^2}} \quad (3.3)$$

By applying the convolution to the normalized image $I_{i,j}$ we get the resulting image $P_{i,j}$.

$$P_{i,j} = \nabla^2 G_{i,j} * I_{i,j} \quad (3.4)$$

$P_{i,j}$ is thus a matrix that contains the second order derivative of the image $I_{i,j}$. A spherical object will cause an edge where the intensity change is similar around a spherical object, but dependent on the distance from the optimal focus. Assuming the Gaussian of the image I is twice differentiable at any point (i, j) , the maximum (or minimum) of the second derivative includes the amplitude of the first derivative at the point where the second derivative is equal to zero, i.e. where the edge is strongest. This can be intuitively understood when considering that if the edge is sharper, the gradient, or first derivative value is larger, and if the gradient value is larger the rate of change, i.e. the second derivative needs to be larger at each side of the edge. Therefore we store a value of the maximum second derivative, $\max(P_{i,j})$, around each analyzed object and use this as a measure of the edge sharpness. This value is then used as input to a calibration function. We also

Chapter 3. Materials and Methods

construct a new binary image Q in which the pixel value $Q_{i,j} = 1$ if any of $|P_{i+1,j} - P_{i,j}|, |P_{i-1,j} - P_{i,j}|, |P_{i,j+1} - P_{i,j}|, |P_{i,j-1} - P_{i,j}| > th$, where $th = 0.002$. $Q_{i,j} = 0$ elsewhere. th is the gradient of the second derivative at the point where the second derivative is zero, i.e. on the edge. Particles are found by searching for closed contours in this binary image.

3.2.3 Comparing Transparent Microspheres and Dots

A spherical lens scatters almost all the incident light in different directions, leaving only a bright spot in the middle where light is transferred directly through. For larger particles in focus, this bright spot will result in a second circular closed contour inside the outer edge.

Small water droplets can be seen as transparent microspheres. The composition changes the refractive index, but this has little effect on the shadow. The outer contour is the same following the same reasoning as with the dots used for calibration [56](Paper I). Diffraction patterns depend on the wavelength of the light and the size of the sphere. The resolution of the constructed system is not high enough for these patterns to be visible.

By using a flood-fill function on the binary image containing the detected contour, starting in a point at a minimum distance from an object, the edge of the filled area will border to the outer contour. This makes it possible to select the outer closed contours of possible particles.

3.2.4 Removing the Center Bright Spot

The center bright spot will make the shadow of a transparent sphere brighter in average than a solid dot. This will have an impact on the size calculation, since the size calculation is based on the shadow impact and the calibration is done using solid dots. Therefore we apply a mask on the image before calculating the size of the shadow. The mask is done by replacing all the centermost pixels in a shape of a circular disc with the intensity of the darkest pixel in the spot. The diameter of the masked disc is the arc length of the edge contour divided by

3.2.5. Measuring Roundness

4π . The bright spot is measured by calculating the difference between the least value and the center pixel. Only particles with a difference larger than 0.1 (ten percent) will have the mask applied

3.2.5 Measuring Roundness

There may be clogs of small microspheres or dust in the samples that are measured. Microspheres, or small water droplets are close to spherical. Therefore we try to exclude all objects that the program find but are not circular. After the detection of object edges, we measure the roundness of each object. A measure of the mean square roundness deviation similar to the one described by ISO [52] can be achieved by calculating the quote between the area of the contour and the square of the total arc length See (equation (3.5)).

$$\text{roundness} = 4\pi \frac{A_{\text{contour}}}{\text{arcLength}^2} \quad (3.5)$$

A_{contour} is the pixel area of the filled contour and arcLength is the perimeter of the measured closed contour. In the calibration and field measurements described, an object is only considered spherical if $\text{roundness} \geq 0.85$.

3.2.6 Light Spectrum

Although water is a good absorber of electromagnetic radiation in most spectral wavelenghts except for the visible, the volume of water droplets is too small for the absorption to be measurable. In visible light, the water droplet can be regarded as a spherical lens with a very short focal length, thus spreading most of the light in diverging directions. Since the used camera is specifically designed for visible and near infrared, we tested and compared two different wavelenghts, 455 nm and 850 nm using the same optical setup. The shorter wavelength gave sharper images.

One would expect diffraction patterns depending on the spectral bandwidth of the light source. The narrower band width the stronger the diffraction would be. A spectrum analyze of the LED showed that the coherence length of the blue LED is about 6.8 μm . Therefore the

Chapter 3. Materials and Methods

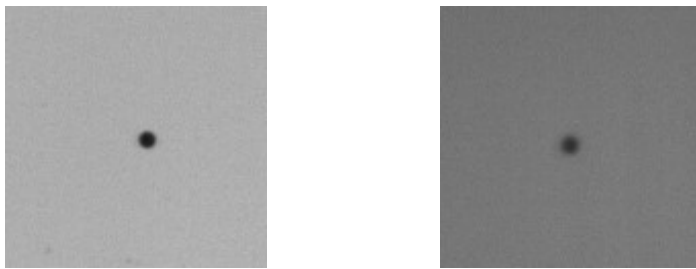


Figure 3.4: Same dot viewed in different background light. 455 nm (left) and 850 nm (right).

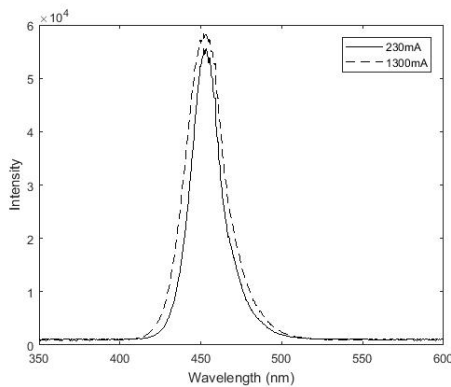


Figure 3.5: Spectrum of the Mightex 455nm LED using two different driving currents. The band width is slightly wider for the higher current.

spectrum was measured using a spectrum analyzer. The result can be seen in Figure 3.5

3.2.7 Laser Light

Using coherent light for imaging means that the effects of interference patterns will dominate the image of small particles. This is e.g. used when reconstructing images in holographic imaging instruments mentioned in section 1.3. Laser illumination was tried using two wavelengths, 450 and 850 nm. The images using laser illuminating the sample from an angle

3.2.8. Image Noise

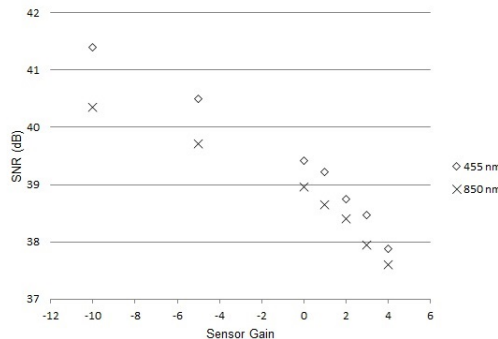


Figure 3.6: SNR for a ten micrometer dot image using two wavelengths and seven gain level settings. Shorter wavelength and lower gain gives less noise.

3.2.8 Image Noise

The total image noise was first measured using the whole image using the 455nm LED light, resulting in a variation coefficient of about nine percent.

The idea came that we should be able to measure the signal to noise relation, if the shadow image of the droplet is represents the signal. This signal to noise ratio (SNR) could possibly be used to increase the accuracy of the measurement. A function was created that calculates the noise level locally around each analyzed droplet image. A correlation could be seen between the SNR and the corresponding measuring range, resulting in an increased sampling volume for higher SNR [56](Paper I). This relation has not been implemented in the LWC calculation for the prototype instrument yet.

The SNR for a ten micrometer dot image was compared for the different available gain level settings in the image sensor. This measurement was done using both the 455 and the 850 nm illumination. The result can be seen in Figure 3.6.

3.2.9 Ambient Light

In daylight, there is always some ambient light. Although the camera is never aimed directly at the sun and the system make use of a

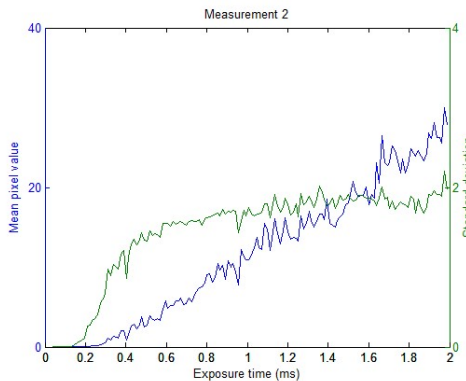


Figure 3.7: Mean pixel value and standard deviation of ambient for a light measurement at 22000 lux.

telecentric lens we wanted to be sure that this light is not enough to affect the measurement. To get an idéa about the amount of ambient light the camera and lens was tested alone in daylight, using a fog generator in front of the lens to reflect light into the lens.

The shortest possible exposure time according to the camera specification is 0.038 ms, slightly depending on other camera settings. For each measurement 152 images were captured, with increasing exposure time from 0.040635 to 1.988535 ms. A delay of 1 second was set between each image. Figure 3.7 shows the mean pixel value and the standard deviation of the value for one of the measurements at 22000 lux ambient light.

Using this setup it was found that an exposure time of at least one second is needed to give a signal that is comparable to the noise level in a normal exposure. In order to image small droplets, the exposure time needs to be less than one μ s, preferably less. This difference is greater than the 8-bit pixel resolution used ($2^8 = 256$).

3.2.10 Light Sensitivity Measurement

The illumination energy required to get a good exposure for each of the eight gain setting levels is shown in Fig. 9. The energy is calculated by using an effectmeter, the area of view and the time that is required for a full exposure. The measurement is described in Paper I. 34 nJ

3.3. Design Considerations

is required for the area in view (7.8 mm^2) for the lowest gain setting, which results in the highest SNR and about 20 nJ for the used setting.

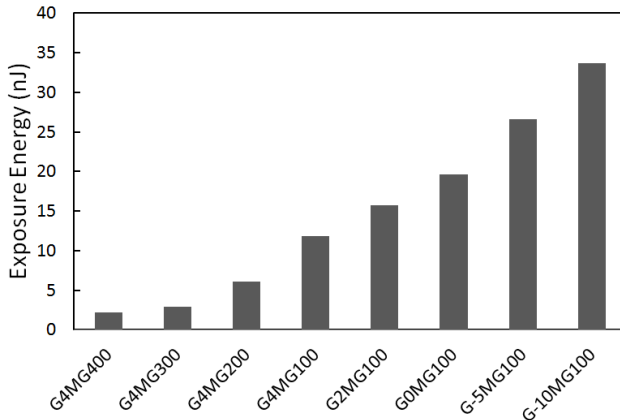


Figure 3.8: Light energy (nJ) for exposure in each of the eight gain levels used. The energy was tuned manually up to a level of high exposure, but not saturating any point in the image.

3.3 Design Considerations

3.3.1 Speed of Light Flash

A value of both MVD and LWC can be derived from a series of images and since the number of measured droplets will depend on the concentration, the accuracy and precision will depend on the number of samples from the total population of droplets.

The illuminative power required to get a good exposure is tested.

3.4 Calibration and Validation of the Calibration

The system is calibrated using a stage micrometer scale with 13 circular dots printed in chrome on a silicon glass. The dots range from 2 to 100 μm in diameter. Each dot is moved linearly in steps of one micrometer in the direction orthogonal to the lenses, thus creating a function where the gradient of the edge depends on the

Chapter 3. Materials and Methods

distance from optimum focus. A threshold on the second derivative gradient strength limits the measured particles to be within a specific measuring range. It is important to select the threshold carefully. If the value of the threshold is too low, there will be many false edges in the image. If it is too high, the measuring range will be too small. The difference between two different thresholds, 0.002 and 0.005 is illustrated by Figure 3.9. The measuring range is here defined as the distance in which the edge detection by Laplacian of Gaussian operator and a threshold makes a closed curve in the resulting binary image.

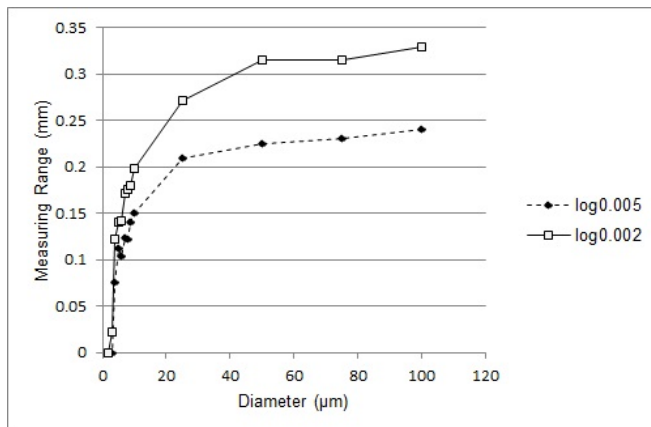


Figure 3.9: Measuring range (mm) vs. diameter for two different thresholds (0.005 and 0.002).

The edge sharpness will affect the position of the edge and the measured shadow slightly. We use the maximum value of the second derivative $P_{i,j}$ for each droplet as a measure of the edge sharpness and include this in the calibration functions, together with the diameter measured from the shadow intensity.

Two second degree approximation surfaces, (3.6) and (3.7), are calculated using the “fit” command in Matlab. z_1 approximates dot diameters from 2 to 10 micrometers and z_2 diameters from 10 to 100 micrometers. x is the maximum second derivative, d^M is the diameter measured from the shadow intensity, p_{xx} and q_{xx} are constants.

3.4.1. Verification of Dot Size

$$z_1 = p_{00} + p_{10}x + p_{01}d^M + p_{20}x^2 + p_{11}xd^M + p_{02}(d^M)^2 \quad (3.6)$$

$$z_2 = q_{00} + q_{10}x + q_{01}d^M + q_{20}x^2 + q_{11}xd^M + q_{02}(d^M)^2 \quad (3.7)$$

By measuring the calibrated microspheres a validation can be made with the expected diameter.

3.4.1 Verification of Dot Size

The dots on the micrometer scale were measured visually using a Leica microscope connected to a digital camera. This was done to get accurate values of the diameter of the dots for use in the calibration. An example image that was measured can be seen in figure 3.10.

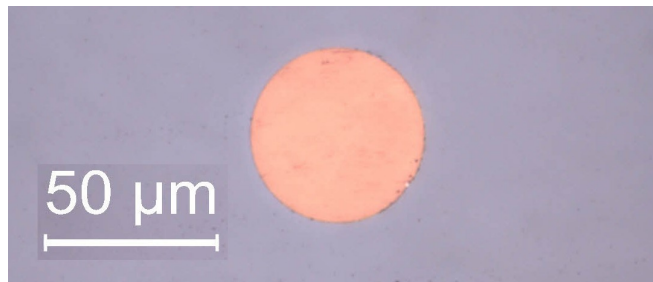


Figure 3.10: The 50 micrometer dot with front illumination imaged using 40x magnifying lens.

This measurement was done using lenses with two different magnifications: 40x and 100x. All the dots average diameters, except the 100 μm dot were found to be within $\pm 0.2 \mu\text{m}$ of their nominal diameter. They are not all perfectly round, but the size accuracy should be good enough to use as calibration reference. The result from this measurement is comprehended in table 3.1.

3.5 The Fog Chamber

The fog chamber is needed to create a test environment for the instrument. Natural fogs tend not to occur outside just when we are ready to test. If possible, it is desirable that the environment can

Nominal Diameter	Di-Excentricity	Diam. 40x	Diam. 100x
5	0.2	5	4.8
6	0.6	5.8	5.8
7	0	7	6.6
8	0	8	7.9
9	0	9	8.8
10	0	10.1	9.8
25	0	24.9	24.7
50	0.4	50.1	49.8
75	0.2	75.2	74.8
100	2.5	100	98.7

Table 3.1: Micro dot verification measurement. All values are in μm . Eccentricity is here the maximum difference in μm between the smallest and the largest measured diameter.

be controlled and verified using a second instrument. It gives an indication of how the instrument will behave in a real measurement. It is also a verification of the instrument's water ingress resistance.

The constructed chamber has a frame made of 30 mm aluminum profiles, fitted with transparent 6 mm polycarbonate walls on all sides using rubber sealing strips. The droplets are produced using an ultrasonic fog generator pushing the droplets to the chamber through a flexible tube approximately 30 mm in diameter and 500 mm long. Next to the fog inlet, there is a dry air inlet with a speed adjustable fan. On the back of the chamber there is a similar sized outlet for air and moisture.

3.6 The Klövsjö Installation

Figure 3.13 shows the installation. On top is the two camera houses of the DII and just below is the smaller CDP. The Lambrecht Eolos weather sensor is seen furthest to the left, mounted on an horizontal boom. In the middle just right of the Eolos is the mobile communication antenna. In the lower center the top of the shortened lattice

3.6. The Klövsjö Installation

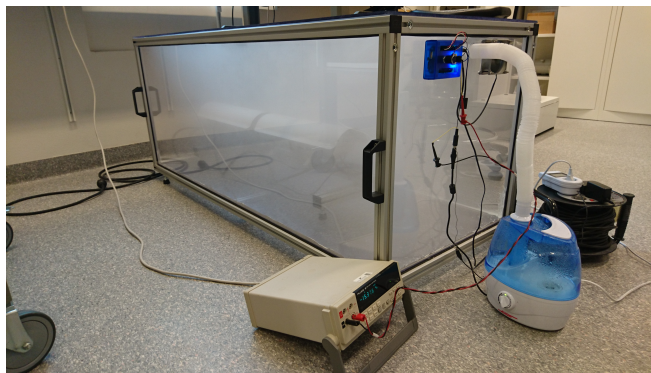


Figure 3.11: Fog chamber with connected droplet generator (blue container) and a multimeter used for fan power measurement. A Beaglebone Black microcontroller (blue box) is used for fan speed regulation.

mast is seen and behind this is the box containing the DII processing computer, the CDP data collection computer and the communications router. The whole installation is about five meters high. An electric servomotor mounted at the base of the pole inside the lattice mast rotates the two instruments automatically to follow the horizontal direction of the wind.

Figure 3.12 shows icing on the front side of the installation.



Figure 3.12: Icing on the front side of the installed instruments.

Chapter 3. Materials and Methods



Figure 3.13: Installation in Klövsjö.

3.7 Numerical Weather Prediction

For a second validation, we carry out weather simulations around the site using the HARMONIE-AROME numerical weather prediction (NWP) model. The model is described in Paper III.

SMHI agreed to run a special model domain locally with 500 meters horizontal resolution for a limited time. The operational forecasts are run at 2.5 km horizontal resolution, and they were used as initial conditions and lateral boundaries for the detailed simulations.

At SMHI, the HARMONIE-AROME model is used for short range operational forecasting. It is run in cooperation with the Norwegian Meteorological Institute. The initial conditions and boundaries for the operational forecasts are provided by the ECMWF global model.

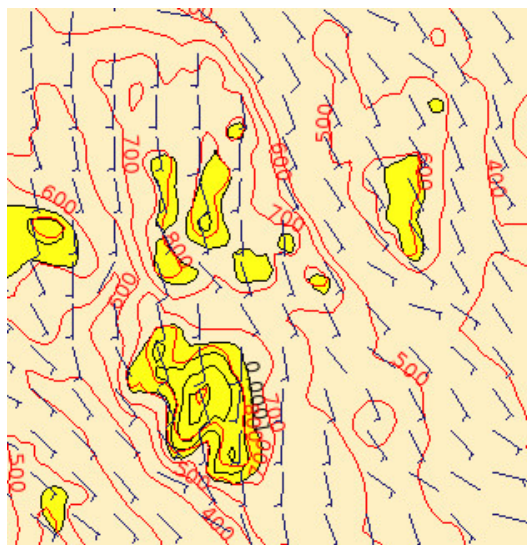


Figure 3.14: Graphical presentation of data from the HARMONIE-AROME weather model covering Klövsjö and the surrounding mountains at a specific point in time using 500 m resolution. Yellow areas are where the model predicts an LWC more than $0.1 \text{ g} \cdot \text{kg}^{-1}$ (Grams of water per kg air.) Simulation and figure by SMHI.

RESULTS

The contents of this chapter are taken from Paper III.

4.1 Measurement of Polymer Microspheres

Four NIST calibrated distributions of microspheres, approximately 5, 10, 20 and 50 μm in diameter were used, resulting in four different measured size distributions. All images were saved and visually inspected, resulting in some measurement outliers due to clogging of smaller particles or contamination of small particles among larger. The outliers that were identified as not of the real distribution are not included in the result shown. Histograms of the measurement can be found in Figure 4.1. A summary of the result is shown in Table 4.1.

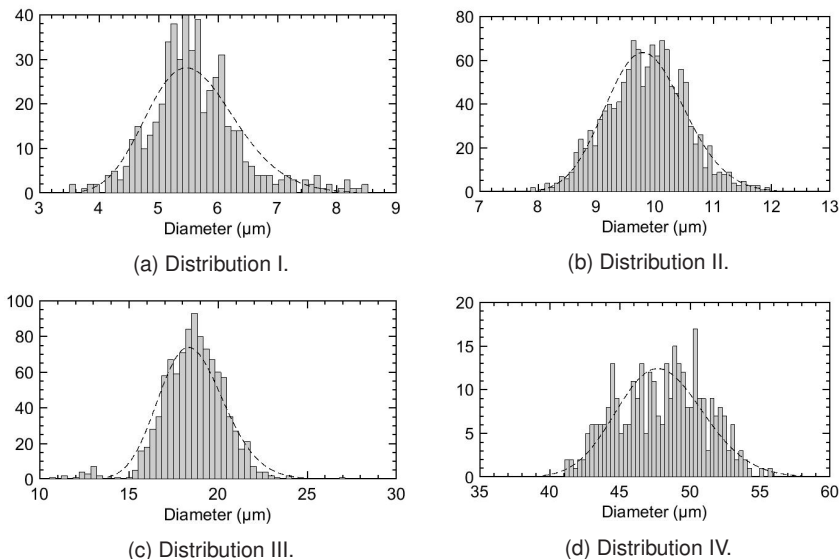


Figure 4.1: Histograms of the four measured distributions. The dashed line is a fitted lognormal of the weighted distribution.

Chapter 4. Results

Distribution	I	II	III	IV	
Stated Diam.	Mean	5.3 (± 0.3)	10.3 (± 0.4)	19.1 (± 0.7)	49.4 (± 1.6)
Measured Mean Diam.		5.6	9.9	18.6	48.0
Stated Std dev	0.5	0.9	1.7	3.5	
Measured Std dev	0.77	0.67	1.7	3.1	

Table 4.1: Summary of the result from the measurement of NIST certified microspheres. All values are in μm .

4.2 Comparison of DII and CDP Data

We compare the instruments by studying the data from 28 February to 1 March. See Figure 4.2 and 4.3. Figure 4.2b shows the LWC measured by the CDP compared with LWC measured by the DII. Using the least square method on the whole data set gives an average quote of 0.27. The quote is drawn in the plot as a straight line from the origin.

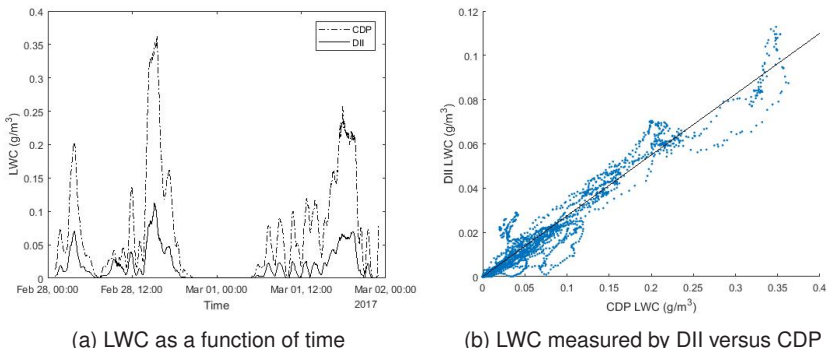


Figure 4.2: LWC measured by the DII and the CDP for 46 hours on 28-02-2017-01-03-2017.

Figure 4.3b shows the MVD measured by the CDP compared with the DII. The least squares method applied on the data set results in a quote of 0.77 and a very small offset of -0.3 μm .

4.2. Comparison of DII and CDP Data

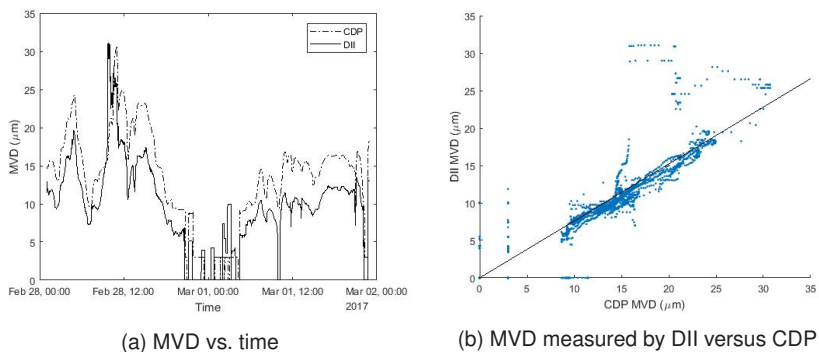


Figure 4.3: MVD minute values measured by the DII and the CDP for 46 hours on 28-02-2017–01-03-2017.

The quote between the LWC values of the two instruments is plotted together with the wind speed in Figure 4.4. The least square average is plotted as a horizontal line at 3.65 (CDP LWC / DII LWC). The logarithmic scale is cropped with 238 quote values above 100 and 121 values below one of a total 2760.

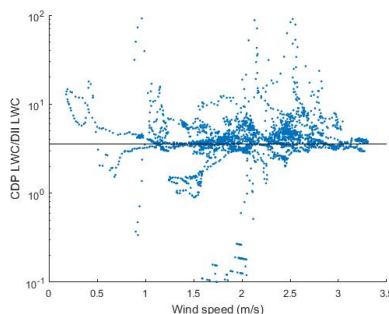


Figure 4.4: Relation between the wind speed and the quote between the LWC measured by the CDP and the DII. The vertical scale is cropped at 1 and 100. 238 values are above 100 and 121 below one out of a total of 2760.

4.3 Comparison of Measured and Modeled Data

Figure 4.5 shows the LWC and the MVD from the two instruments compared with the data from the HARMONIE-AROME model at 500 m resolution. The fog lasted for about 19 hours on 12-11-2016. The difference between the two instruments follows the same systematic pattern as for other occasions. The HARMONIE-AROME model data of the LWC follows the general data of the LWC but fails to detect the large increase in LWC between 05:00 and 12:00. The predicted MVD of the model is closer to the actual values of the DII than the CDP.

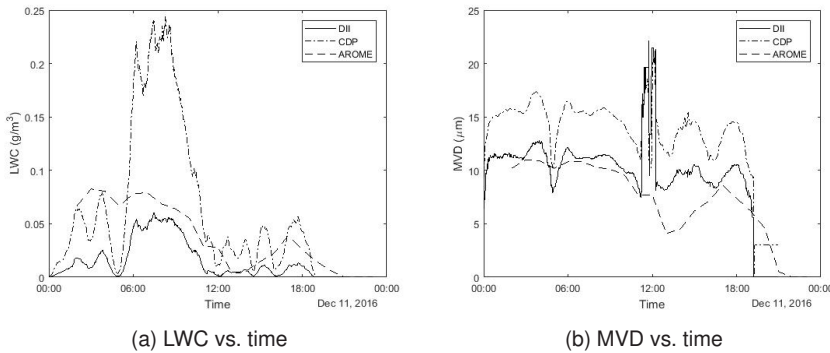


Figure 4.5: LWC and MVD measured by the DII and the CDP 11-12-2016. HARMONIE-AROME model data using 500 meter resolution.

Figure 4.6 shows the result from measurement 03-02-2017–06-02-2017. Unfortunately no data from the CDP was saved from this occasion due to a full memory. The double spike in the MVD diagram 4.6b at 04:17 and 04:41 on 05-02-2017 is mainly caused by two droplets, 51 and 74 µm (see Figure 5.1) in combination with a number of large droplets between 30 and 40 µm in diameter.

4.3. Comparison of Measured and Modeled Data

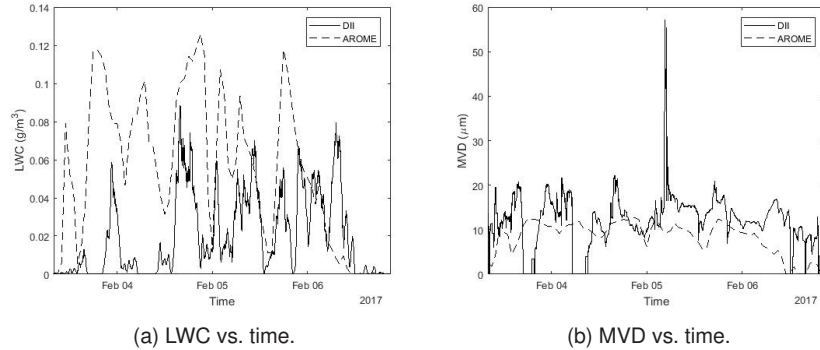


Figure 4.6: LWC and MVD measured 03-02-2017–06-02-2017 by the DII. HARMONIE-AROME model data using 2.5 km resolution, stored every 60 minutes.

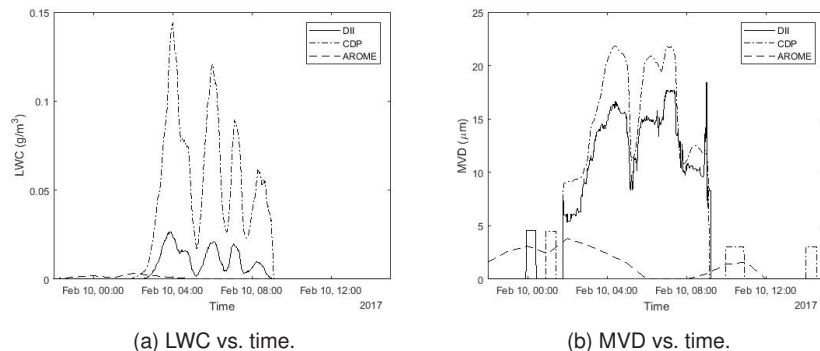


Figure 4.7: LWC and MVD measured by the DII and the CDP 10-02-2017. HARMONIE-AROME model data using 2.5 km resolution, stored every 60 minutes.

— Chapter 5 —

DISCUSSION

5.1 Starting Studies

5.1.1 *Infrared and Visible Light*

The amount of absorbed light in a small water droplet is close to negligible compared to the scattered light. In a large ensemble of droplets, such as a cloud, the total absorption will still be significant, especially for wavelengths in the near and far infrared. Since it was possible, we made a quick comparison of illumination using blue light (ca 450nm) and near infrared (ca 850nm). The blue light gave the sharpest image, probably due to the sensor's slightly higher sensitivity for blue light. But also possibly due to the higher theoretical resolving power as described by Rayleigh's criterion. See Paper I.

5.1.2 *Laser Light*

Lasers are used in most optical instruments for droplet measurement and for many good reasons. Prices for high power semiconductor lasers have also become very attractive. The coherency gives the possibility of using holographic reconstruction of diffraction patterns to achieve a larger measuring range than what is possible in conventional imaging. Sizing of particles may still be tricky, and especially more calculation intensive. For conventional imaging of small particles the coherence mainly causes problems as the diffraction patterns will be strong and visible. Although it is possible to make the laser incoherent e.g. by using diffusers or optical fibres it is still another circumstance that makes the complete system slightly more complex.

5.1.3 *Image Noise and SNR*

The design using a weakly collimated LED that illuminates an area slightly larger than the field of view makes the system quite insensitive to misalignment of the camera and the light source. Temporal or

Chapter 5. Discussion

permanent changes in light intensity caused by a minor misalignment can be automatically compensated for by continuous measurement of the total exposure level. If the level of exposure is increasing or decreasing, the length of the light pulse is changed correspondingly. The light intensity can also be affected by dirt on the front glass of the housings.

Spatial dissimilarities in the light intensity that are not caused by noise we can compensate for by calculating the local average intensity of the background around each measured droplet. The size of a droplet is then based on the intensity dip caused by the shadow compared with its local background.

5.1.4 Image Pre-processing

To increase the number of processed images a pre-process is done using a variable threshold as described in section 3.2. The processing speed could be increased even more limiting the edge detection algorithm to the region or regions around the discovered differences.

5.1.5 Light Sensitivity Measurement

This measurement was done to get an idea about the theoretical minimum amount of energy required for each image. In practice, the light from the collimated LED used will be spread so that only a small part of the total emitted energy actually reaches the sensor. The area in view is about 8 times smaller than the illuminated area of the collimated LED, which was measured to about 8x8 mm. Also a lot of the light energy will be absorbed in the telecentric lens.

5.1.6 Speed of Light Flash

the illuminative power need to be enough to get a good exposure at a high wind speeds. The LED used was fully functional after four months of continuous measurements using 12 times higher current than specified. Using even higher current

5.2 Aerodynamics

Many existing instruments suffer from errors caused by the instrument itself during sampling, e.g. when droplets get stuck on the inlet or shatters into smaller droplets. The DII is not as small and aerodynamically shaped as the CDP, therefore a difference between the instruments would be expected depending on the air speed. However, a comparison between the measured values of LWC showed no connection between the wind speed and the difference in the measured LWC. The wind speed during the comparison was only $1\text{--}4 \text{ m} \cdot \text{s}^{-1}$ which probably explain why the less aerodynamic shape of the DII compared with the CDP has no noticeable effect. This could change dramatically when measuring at higher wind speeds.

5.3 Difficulties with Polymer Microspheres

To get a second verification of the sizing algorithm we made a measurement using polymer microspheres of known calibrated size distributions.

5.3.1 Speed

5.3.2 Clogging

Small microspheres are forming larger clogs that are measured as single microspheres. The reason may be static electricity or humidity. As can be seen in the five micrometer measurement, the result of some clogs becomes outliers in the expected distribution. This needs to be considered when solid microspheres are used as reference objects. Colliding liquid water droplets would of course coalesce into larger droplets, thereby changing the diameter.

The equipment and the dispenser was thoroughly cleaned using compressed air between each measurement. Still there may be microspheres or other contamination left, changing the distribution slightly.

discuss
the speed
needed for
the purpose
- measuring
ice

Chapter 5. Discussion

Measured mean and standard deviation of all distributions were found to be within the stated calibrated values. This can be seen as a confirmation that the instrument calibrated only by the micrometer dot scale is measuring the microsphere samples correctly.

5.3.3 *Roundness*

A perfectly circular disc measured using an infinite resolution would have an expected roundness value equal to one. In practice, this is not possible to achieve in a digital image. But the contour is only used as detection criteria. Instead, the diameter is calculated using the negative shadow intensity. Therefore the contour roundness itself should not have very large impact on the accuracy.

The roundness criteria according to ISO [52] set at 0.85 in this measurement seems to work fine. It excludes most irregular objects, like clogs in the five micrometer measurement. When measuring fogs in cold climates, the water droplets will be mixed with ice crystals. While larger crystals will mostly be sorted out by the roundness criteria, crystals smaller than ten micrometer may be difficult, and five micrometer crystals more or less impossible to distinguish from liquid water droplets unless very different in shape.

5.3.4 *Calibration Validation*

The calibration functions derived from the measurement of known sized dots is an approximation and an interpolation. It is based on the assumption that light scatters similarly on the edge independently of the size of the object. This is not quite true, especially for smaller particles [7]. For particles around ten micrometer or less in diameter we would expect different intensities forming a diffraction pattern close to the edge. The pattern would be stronger the more coherent the illumination. In this system, using LED illumination, the coherence length is short enough that no patterns are visible. Still changes to the edge for the smallest diameters can still not be altogether ruled out.

The experiment using calibrated spheres confirms that the measurement of droplet diameters is accurate. It is however not a confirmation of the measurement volume [57] since we do not know

the concentration of the microspheres. This means that we cannot yet confirm an accurate measurement of the LWC. To do that, an independent verification of the measurement volume is needed.

5.4 LED Illumination

Using a high power LED instead of laser reduces the interference effects used in e.g. holography [26], but since it is a monochromatic source, interference may not be completely ruled out. The coherence length for the blue LED is calculated in Paper I.

LEDs can sometimes be used with currents far above the specifications, as long as the pulse length is short and the duty cycle is low enough to permit the heat generated to be transported away between the pulses. Using the LED above specifications may though affect the efficiency and aging of the LED. LED emittance also depends on the temperature. Depending on the capacitance of the diode, the rise time may limit the current, although there exist some techniques to shorten the LED pulses [63, 67].

The LED used was fully functional after four months of continuous measurements using 12 times higher current than specified. At 12 ampere driving current, the flash duration could be lowered to approximately 250 ns, still using the normal settings of amplification in the camera. Using even higher current would lower the flash duration still. A question is how high current the LED can handle and how the lifetime is affected by driving higher currents through.

5.5 Statistics

A value of both MVD and LWC can be derived from a series of images and since the number of measured droplets will depend on the concentration, the accuracy and precision will depend on the number of samples from the total population of droplets.

5.6 Droplets and Size Distributions

Droplets that are very close are likely to coalesce, thereby decreasing the number concentration at a rate that appears to increase for larger droplets and more complex droplet size distributions [8].

Due to the small depth of the measurement volume, i.e. the measuring range compared with the field of view, the likelihood of finding two droplets very close in the image is very low due to the low number concentration of droplets we are measuring. A solution is to make a measurement of the droplet's circularity and add this as selection criteria for the measurement. This solution also works as a filter for ice or snow particles.

The drop size distribution of cloud droplets 3-50 μm in diameter have usually been considered to follow a lognormal or gamma curve [50, 43, 59]. This also applies to rain [66]. However, more recent measurements of drop size distributions show that the distribution greatly varies [31, 60, 54, 11]. Consequently, the results will depend on the measurement method and the sampling volume.

5.6.1 Sampling Speed and Volume

Since the DII has no external trigger of the imaging, the sampling speed, i.e. the volume of air and droplets that is scanned per time unit, depends on the measuring volume of each image and the imaging speed.

The sampling speed of the CDP is linearly dependent on the wind speed. The sample area also depends on the size of the measured droplets, but the factory calibration value is given for all sizes. The sampling speed of the DII depends primarily on the image frame rate and the measurement range for each droplet size. At a wind speed of 2 m/s, the sampling speed of the CDP is $4.1 \cdot 10^{-7} \text{ m}^3 \cdot \text{s}^{-1}$. This is 39 times higher than the sampling speed of the DII for 20 μm particles. To achieve the same sampling speed, the frame rate of the DII would need to be almost 200 s^{-1} .

Despite the relatively low sampling speed and the small sampling volume of the DII, it seems that by averaging the LWC and the MVD over a period of 30 minutes, enough precision is achieved to be able to compare the two instruments. Since the purpose of the DII is primarily to detect conditions for icing on wind turbines, and provide in-situ observational data for NWP models, the achieved sampling speed may even be good enough, at least for the latter. If the speed is good enough to decide when to switch on de-icing on the blades

5.6.2. Large Droplets

depends on how quickly the ice builds up, and what de-icing method is used. During icing, high LWC and high MVD are expected.

When comparing the 30 min moving average values for the period 28 February – 1 March, shown in Figure 4.2a and Figure 4.3a, there is very good agreement between the curves, with the exception of 11.30-12.00 when at least ten droplets 25-35 μm in diameters were measured by the DII, resulting in a significantly higher MVD and LWC measured by the DII than the CDP. The reason why the CDP did not measure any similarly sized particles on this particular occasion is not known. There is also a difference in the MVD when the LWC is very low resulting in a small number of measured droplets.

The sampling speed could be raised by e.g. changing the optical magnification but then at the cost of a lower optical resolving power. Different ideas to increase the sampling speed of the DII are discussed in Paper I and Paper II.

Another way of increasing the sampling speed is to increase the imaging speed. Cameras with a high imaging speed exist and the flash pulse is so short that it would still be a low duty cycle for the LED. The most limiting factor is probably the processing time. This can be solved by implementing parts of the image processing in hardware.

The speed requirement finally depends on the application. If the instrument is used for the verification of NWP models, the sampling speed of the prototype may be enough. If the instrument is supposed to be used for triggering de-icing, the sampling speed may need to be increased.

5.6.2 *Large Droplets*

The CDP does not measure particles larger than 50 μm . But if the distribution of droplets was following a lognormal, or gamma curve [50, 43] also for particles larger than 50 μm , enough large droplets should have been detected by the CDP to see an increase in the measured MVD. As demonstrated, this was not always the case. A possible explanation is that the larger cloud droplets do not follow the lognormal distribution when they are above a certain size. If this is true, the predicted MVD may be less useful for the description of a cloud aerosol distribution, as well as for conclusions about possible

icing. In the case with supercooled large droplets, the LWC may be more important to measure than the MVD. But to fully understand this, a parallel measurement using an ice load instrument is required.

Figure 5.1 and Figure 5.2 show supercooled large droplets measured during the fog on 05-02-2017.

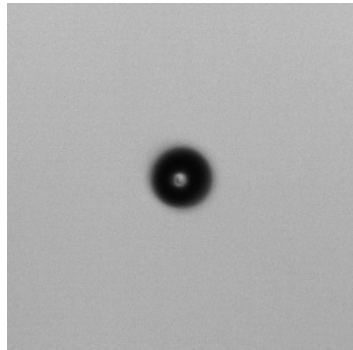


Figure 5.1: A $74 \mu\text{m}$ droplet detected at 04:41 on 05-02-2017.

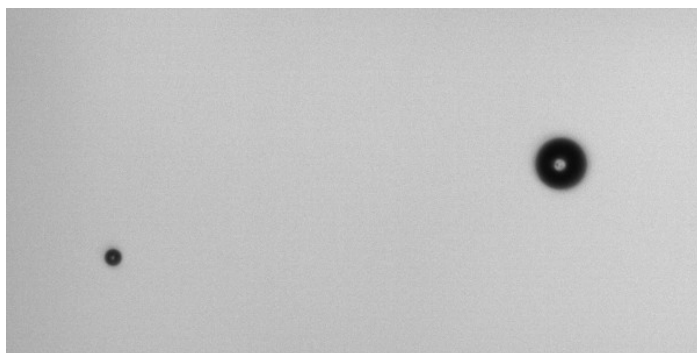


Figure 5.2: Two droplets, 19 and $62 \mu\text{m}$ in diameter detected in the same image at 16:48 on 05-02-2017.

5.7 Icing

The risk of icing increases with increasing wind speed [45].

During the field study there were several instances when the LWC and MVD was high enough to lead to icing. A study to further

investigate the connection between these parameters and the ice load according to ISO 12494 [46] should be carried out. An ice monitoring device, like the Combitech IceMonitor [20, 65] can be used for this. This should preferably be done in combination with a third independent LWC and MVD measurement, e.g. by using rotating cylinders [44, 34]. A heated hygrometer measuring the true water content (TWC) can be used as an alternative verification of the LWC measurement when all the atmospheric water is in liquid form [62].

SUMMARY OF THE THESIS

The thesis describes the work resulting in three scientific papers.

6.1 General Conclusions

Shadowgraph imaging can be used for comparison and validation of NWP models. The technique can also be used for size reference measurement of instruments based on other techniques. The accuracy of the particle size measurement is high.

The accuracy of the concentration measurement is questioned due to the systematic difference to the reference instrument, but has the potential to become high due to the single-particle measurement range calibraiton. The precision of the instrument depends mainly on the number of images that is used to achieve each measurement value.

The real-time performance of the instrument is limited by the image retrieval and processing speed and depends on the precision required.

6.2 Other Conclusions

1. The test using polymer microspheres confirms that the DII, calibrated by a micrometer dot scale measures the size of the tested samples correctly. The size distributions achieved by this instrument are within the tolerances specified by the manufacturer of the microspheres.
2. The used LED is capable of emitting light at much higher currents than the specified maximum.
3. The DII was proven to withstand and function in a very humid environment.
4. The LWC in a fog chamber can be controlled by regulating the fan speed and the power of an ultrasonic humidifier.

5. Both the CDP and the DII make precise measurements of the LWC using a 30 minute average window. Supercooled droplets with diameters above 50 μm exist in fogs where MVD is lower than predicted.
6. The CDP achieves higher values of the droplet diameters compared with the DII. This leads to an even higher difference in the measured LWC.
7. A better calibration of the measurement range depending on the spatial position of the measured particle, the lighting condition or the SNR is needed to get a better estimation of the measurement volume.
8. The predicted LWC and MVD data from HARMONIE-AROME have better agreement with the measured values when using a 500 meter horizontal resolution than the usual 2.5 km resolution.
9. The DII proved to be fully operational without site attendance for four months of continuous measurement. The instrument speed and resolution seems to be good enough to detect and measure the conditions for icing. The data can be used to verify and validate NWP models.
10. Large droplets are important to understand the total size distribution of liquid water droplets and may play an important role during icing.

6.3 Future Work

1. A new study of the measurement range should be done including e.g. spatial position, lighting condition and SNR.
2. A simultaneous measurement of ice load should be done to find out more about the relationship between MVD, LWC and ice load.
3. The DII should be improved by increasing the image processing speed. This can be done e.g. by implementing pre-processing

6.4. Authors' Contributions

algorithms in hardware or by switching to a more powerful processing computer.

4. Higher wind speeds can be used. The LED flash can be shortened by using higher. This means changing the hardware that drives the LED to achieve a higher current.
5. A study to further investigate the relation between the different parameters impact on the ice load may be done using the instruments an ice monitoring device. This should be done in combination with a third independent LWC and MVD measurement, e.g. by using rotating cylinders[44].

6.4 Authors' Contributions

Contributions from the authors and others are summarized in the table below.

Chapter 6. Summary of the Thesis

Contributor	Paper I	Paper II	Paper III
Staffan Rydholm	MA		Survey of existing instruments and techniques for droplet measurement. Problem formulation. Estimation of the optical limitations for measurement. Choise of technique for imaging. Choise of image processing method and implementation in Matlab. Laboratory setup and method of calibration. Statistical analysis of precision.
		MA	Design and integration of the instrument and the fog chamber. Implementation of the real time measurement and analysis program in Linux/C++ with OpenCV. Measurement of polymer microspheres as reference objects. Measurement of a fog using the instrument inside the developed fog chamber and flow control.
		MA	Integration of the DII for real world measurements. Choise of reference instrument. Optimization of the measurement and analysis application. Commissioning of the DII on site and supervision of the data collection.
Benny Thörnberg	CA		Supervision of the work, oral discussions and advice about methods, optics and statistics. Discussion regarding the fourier analysis of a theoretical model of a droplet.
		CA	Supervision of work. Integration of the power module for the LED flash.
		CA	Supervision. Choise of mechanics and motor for the rotation. Commissioning on site.
Esbjörn Olsson SMHI	PM		System requirements discussion and analysis.
		CA	Choise of measurement site. Theory of NWP models and implementation of the high resolution model. Weather simulations.
		PM	Project leader at Combitech and commissioning on the measurement site.
Patrik Jonsson Combitech		PM	Mechanical integration of the complete rotational system on the mast and commissioning on site.
		PM	Setup and commissioning of the CDP data logging unit.
Lisa Velander	LC	LC	

Table 6.1: MA = Main Author, CA = Co-Author, PM = Project Member, LC = Language Check.

BIBLIOGRAPHY

- [1] Ceyhun Akcay, Pascale Parrein, and Jannick P Rolland. "Estimation of longitudinal resolution in optical coherence imaging". In: *Applied optics* 41.25 (2002), pp. 5256–5262.
- [2] Albert Ansmann, Maren Riebesell, and Claus Weitkamp. "Measurement of atmospheric aerosol extinction profiles with a Raman lidar". In: *Optics letters* 15.13 (1990), pp. 746–748.
- [3] D. Baumgardner. "An Analysis and Comparison of 5 Water Droplet Measuring-Instruments". In: *Journal of Climate and Applied Meteorology* 22.5 (1983), pp. 891–910.
- [4] D. Baumgardner et al. "Airborne instruments to measure atmospheric aerosol particles, clouds and radiation: A cook's tour of mature and emerging technology". In: *Atmospheric Research* 102.1-2 (2011), pp. 10–29.
- [5] D Baumgardner et al. "The cloud, aerosol and precipitation spectrometer: a new instrument for cloud investigations". In: *Atmospheric research* 59 (2001), pp. 251–264.
- [6] Hans Bergström et al. *Wind power in cold climates: Ice mapping methods*. Elforsk AB, 2013.
- [7] Craig F Bohren and Donald R Huffman. *Absorption and scattering of light by small particles*. John Wiley & Sons, 2008.
- [8] Róbert Bordás et al. "Droplet collisions and interaction with the turbulent flow within a two-phase wind tunnel". In: *Physics of Fluids (1994-present)* 23.8 (2011), p. 085105.
- [9] Rolv Erlend Bredesen et al. *IEA Wind Recommended Practices 13, Edition 2: Wind Energy Projects in Cold Climates*. Tech. rep. 2017.
- [10] John Canny. "A computational approach to edge detection". In: *Pattern Analysis and Machine Intelligence, IEEE Transactions on* 6 (1986), pp. 679–698.

Bibliography

- [11] Stewart G Cober and George A Isaac. "Characterization of aircraft icing environments with supercooled large drops for application to commercial aircraft certification". In: *Journal of Applied Meteorology and Climatology* 51.2 (2012), pp. 265–284.
- [12] Stewart G Cober, George A Isaac, and J Walter Strapp. "Characterizations of aircraft icing environments that include supercooled large drops". In: *Journal of Applied Meteorology* 40.11 (2001), pp. 1984–2002.
- [13] Ruben D Cohen. "Shattering of a liquid drop due to impact". In: *Proceedings of the Royal Society of London A: Mathematical, Physical and Engineering Sciences*. Vol. 435. The Royal Society, 1991, pp. 483–503.
- [14] Paul J. Connolly et al. "Calibration of the Cloud Particle Imager Probes Using Calibration Beads and Ice Crystal Analogs: The Depth of Field". In: *Journal of Atmospheric and Oceanic Technology* 24.11 (2007), pp. 1860–1879.
- [15] N Dalili, A Edrisy, and R Carriveau. "A review of surface engineering issues critical to wind turbine performance". In: *Renewable and Sustainable Energy Reviews* 13.2 (2009), pp. 428–438.
- [16] S Dierer, R Oechslin, and R Cattin. "Wind turbines in icing conditions: performance and prediction". In: *Advances in Science and Research* 6 (2011), p. 245.
- [17] James E Dye and Darrel Baumgardner. "Evaluation of the forward scattering spectrometer probe. Part I: Electronic and optical studies". In: *Journal of Atmospheric and Oceanic Technology* 1.4 (1984), pp. 329–344.
- [18] Jordi Estevadeordal and Larry Goss. "PIV with LED: particle shadow velocimetry (PSV)". In: *43rd AIAA aerospace sciences meeting and exhibit, meeting papers*. 2005, pp. 12355–12364.
- [19] PR Field, AJ Heymsfield, and A Bansemer. "Shattering and particle interarrival times measured by optical array probes in ice clouds". In: *Journal of Atmospheric and Oceanic Technology* 23.10 (2006), pp. 1357–1371.

- [20] S Fikke et al. "COST 727: Atmospheric Icing on structures". In: *Measurements and data collection on icing: State of the Art, Publication of MeteoSwiss* 75.110 (2006), pp. 1422–1381.
- [21] Karen J Finstad, Edward P Lozowski, and Lasse Makkonen. "On the median volume diameter approximation for droplet collision efficiency". In: *Journal of the atmospheric sciences* 45.24 (1988), pp. 4008–4012.
- [22] Rafael C Gonzales and Richard E Woods. *Digital Image Processing, 2-nd Edition*. 2002.
- [23] Gösta H Granlund. "Fourier preprocessing for hand print character recognition". In: *IEEE transactions on computers* 100.2 (1972), pp. 195–201.
- [24] George M Hale and Marvin R Querry. "Optical constants of water in the 200-nm to 200- μm wavelength region". In: *Applied optics* 12.3 (1973), pp. 555–563.
- [25] Yiqiang Han, Jose Palacios, and Sven Schmitz. "Scaled ice accretion experiments on a rotating wind turbine blade". In: *Journal of Wind Engineering and Industrial Aerodynamics* 109 (2012), pp. 55–67.
- [26] J Henneberger et al. "HOLIMO II: a digital holographic instrument for ground-based in situ observations of microphysical properties of mixed-phase clouds". In: *Atmospheric Measurement Techniques* 6.11 (2013), pp. 2975–2987.
- [27] Matthew C. Homola, Per J. Nicklasson, and Per A. Sundsbø. "Ice sensors for wind turbines". In: *Cold Regions Science and Technology* 46.2 (2006), pp. 125–131.
- [28] Matthew C. Homola et al. "Effect of atmospheric temperature and droplet size variation on ice accretion of wind turbine blades". In: *Journal of Wind Engineering and Industrial Aerodynamics* 98.12 (2010), pp. 724–729.
- [29] Matthew C Homola et al. "Performance losses due to ice accretion for a 5 MW wind turbine". In: *Wind Energy* 15.3 (2012), pp. 379–389.

Bibliography

- [30] Robert F Ide. *Comparison of Liquid Water Content Measurement Techniques in an Icing Wind Tunnel*. Tech. rep. DTIC Document, 1999.
- [31] AR Jameson and AB Kostinski. "What is a raindrop size distribution?" In: *Bulletin of the American Meteorological Society* 82.6 (2001), pp. 1169–1177.
- [32] William J Jasinski et al. "Wind turbine performance under icing conditions". In: *Journal of Solar Energy Engineering* 120.1 (1998), pp. 60–65.
- [33] Ville A Kaikkonen, Dmitry Ekimov, and Anssi J Makynen. "A holographic in-line imaging system for meteorological applications". In: *IEEE Transactions on Instrumentation and Measurement* 63.5 (2014), pp. 1137–1144.
- [34] Daniel Knezevici, Richard Kind, and Myron Oleskiw. "Determination of Medium Volume Diameter (MVD) and Liquid Water Content (LWC) by Multiple Rotating Cylinders". In: *43rd AIAA Aerospace Sciences Meeting and Exhibit*. 2005, p. 861.
- [35] Robert G Knollenberg. "The optical array: An alternative to scattering or extinction for airborne particle size determination". In: *Journal of Applied Meteorology* 9.1 (1970), pp. 86–103.
- [36] AV Korolev, JW Strapp, and GA Isaac. "Evaluation of the accuracy of PMS optical array probes". In: *Journal of Atmospheric and Oceanic Technology* 15.3 (1998), pp. 708–720.
- [37] AV Korolev et al. "Evaluation of measurements of particle size and sample area from optical array probes". In: *Journal of Atmospheric and Oceanic Technology* 8.4 (1991), pp. 514–522.
- [38] Linhong Kou, Daniel Labrie, and Petr Chylek. "Refractive indices of water and ice in the 0.65-to 2.5- μm spectral range". In: *Applied optics* 32.19 (1993), pp. 3531–3540.
- [39] Bjørn Egil Kringlebotn Nygaard, Jón Egill Kristjánsson, and Lasse Makkonen. "Prediction of In-Cloud Icing Conditions at Ground Level Using the WRF Model". In: *Journal of Applied Meteorology and Climatology* 50.12 (2011), pp. 2445–2459.

- [40] Thomas Kuhn, Igor Grishin, and JJ Sloan. "Improved imaging and image analysis system for application to measurement of small ice crystals". In: *Journal of Atmospheric and Oceanic Technology* 29.12 (2012), pp. 1811–1824.
- [41] Pramod Kulkarni, Paul A Baron, and Klaus Willeke. *Aerosol measurement: principles, techniques, and applications*. John Wiley & Sons, 2011.
- [42] RP Lawson and RH Cormack. "Theoretical design and preliminary tests of two new particle spectrometers for cloud microphysics research". In: *Atmospheric research* 35.2 (1995), pp. 315–348.
- [43] Seungwon Lee, Brian H Kahn, and João Teixeira. "Characterization of cloud liquid water content distributions from CloudSat". In: *Journal of Geophysical Research: Atmospheres* 115.D20 (2010).
- [44] L. Makkonen. "Analysis of Rotating Multicylinder Data in Measuring Cloud-Droplet Size and Liquid Water-Content". In: *Journal of Atmospheric and Oceanic Technology* 9.3 (1992), pp. 258–263.
- [45] Lasse Makkonen. "Models for the growth of rime, glaze, icicles and wet snow on structures". In: *Philosophical Transactions of the Royal Society of London A: Mathematical, Physical and Engineering Sciences* 358.1776 (2000), pp. 2913–2939.
- [46] Lasse Makkonen, Pertti Lehtonen, and Mika Hirviniemi. "Determining ice loads for tower structure design". In: *Engineering Structures* 74 (2014), pp. 229–232.
- [47] Lasse Makkonen et al. "Modelling and prevention of ice accretion on wind turbines". In: *Wind Engineering* 25.1 (2001), pp. 3–21.
- [48] David Marr and Ellen Hildreth. "Theory of edge detection". In: *Proceedings of the Royal Society of London. Series B. Biological Sciences* 207.1167 (1980), pp. 187–217.
- [49] Gustav Mie. "Beiträge zur Optik trüber Medien, speziell kolloidaler Metallösungen". In: *Annalen der physik* 330.3 (1908), pp. 377–445.

Bibliography

- [50] Natasha L Miles, Johannes Verlinde, and Eugene E Clothiaux. "Cloud droplet size distributions in low-level stratiform clouds". In: *Journal of the atmospheric sciences* 57.2 (2000), pp. 295–311.
- [51] B. E. K. Nygaard, J. E. Kristjansson, and L. Makkonen. "Prediction of In-Cloud Icing Conditions at Ground Level Using the WRF Model". In: *Journal of Applied Meteorology and Climatology* 50.12 (2011), pp. 2445–2459.
- [52] International Standardization Organization. ISO 12181-1: 2011, *Geometrical Product Specifications (GPS)-Roundness-Part 1: Vocabulary and parameters of roundness*. 2011.
- [53] Olivier Parent and Adrian Ilinca. "Anti-icing and de-icing techniques for wind turbines: Critical review". In: *Cold regions science and technology* 65.1 (2011), pp. 88–96.
- [54] Gerhard Peters et al. "Profiles of raindrop size distributions as retrieved by microrain radars". In: *Journal of applied meteorology* 44.12 (2005), pp. 1930–1949.
- [55] T Reisinger et al. "On the relative intensity of Poisson's spot". In: *New Journal of Physics* 19.3 (2017), p. 033022.
- [56] Staffan Rydholm and Benny Thornberg. "Liquid Water Content and Droplet Sizing Shadowgraph Measuring System for Wind Turbine Icing Detection". In: *IEEE Sensors Journal* 16.8 (2015), pp. 2714–2725.
- [57] Staffan Rydholm and Benny Thörnberg. "Droplet imaging instrument metrology instrument for icing condition detection". In: *Imaging Systems and Techniques (IST), 2016 IEEE International Conference on*. IEEE, 2016, pp. 71–76.
- [58] Wayne R Sand et al. "Icing conditions encountered by a research aircraft". In: *Journal of climate and applied meteorology* 23.10 (1984), pp. 1427–1440.
- [59] John H Seinfeld, Spyros N Pandis, and Kevin Noone. *Atmospheric chemistry and physics: from air pollution to climate change*. 1998.
- [60] RA Shaw, AB Kostinski, and ML Larsen. "Towards quantifying droplet clustering in clouds". In: *Quarterly journal of the royal meteorological society* 128.582 (2002), pp. 1043–1057.

- [61] Jaiwon Shin and Thomas H Bond. *Results of an icing test on a NACA 0012 airfoil in the NASA Lewis Icing Research Tunnel*. National Aeronautics and Space Administration, 1992.
- [62] J. K. Spiegel et al. "Evaluating the capabilities and uncertainties of droplet measurements for the fog droplet spectrometer (FM-100)". In: *Atmospheric Measurement Techniques* 5.9 (2012), pp. 2237–2260.
- [63] Hiroyuki Tanaka, Yohtaro Umeda, and Osamu Takyu. "High-speed LED driver for visible light communications with drawing-out of remaining carrier". In: *Radio and Wireless Symposium (RWS), 2011 IEEE*. IEEE, 2011, pp. 295–298.
- [64] Gregory Thompson et al. "Using the Weather Research and Forecasting (WRF) model to predict ground/structural icing". In: *13th International Workshop on Atmospheric Icing on Structures, METEOTEST, Andermatt, Switzerland*. 2009.
- [65] Petra Thorsson, Stefan Söderberg, and Hans Bergström. "Modelling atmospheric icing: A comparison between icing calculated with measured meteorological data and NWP data". In: *Cold Regions Science and Technology* 119 (2015), pp. 124–131.
- [66] Carlton W Ulbrich. "Natural variations in the analytical form of the raindrop size distribution". In: *Journal of Climate and Applied Meteorology* 22.10 (1983), pp. 1764–1775.
- [67] Omar Veledar et al. "Simple techniques for generating nanosecond blue light pulses from light emitting diodes". In: *Measurement Science and Technology* 18.1 (2007), p. 131.
- [68] Timothy P Wallace and Paul A Wintz. "An efficient three-dimensional aircraft recognition algorithm using normalized Fourier descriptors". In: *Computer Graphics and Image Processing* 13.2 (1980), pp. 99–126.
- [69] AD Ward, M Zhang, and O Hunt. "Broadband Mie scattering from optically levitated aerosol droplets using a white LED". In: *Optics express* 16.21 (2008), pp. 16390–16403.

Bibliography

- [70] Manfred Wendisch and Jean-Louis Brenguier. *Airborne measurements for environmental research : methods and instruments*. Wiley Series in Atmospheric Physics and Remote Sensing. Weinheim: Wiley-VCH, 2013.
- [71] CD Westbrook et al. "Estimating drizzle drop size and precipitation rate using two-colour lidar measurements". In: *Atmospheric Measurement Techniques* 3.3 (2010), pp. 671–681.
- [72] C. Willert et al. "Pulsed operation of high-power light emitting diodes for imaging flow velocimetry". In: *Measurement Science and Technology* 21.7 (2010), p. 075402.